TRIPURARI DAS GUPTA[1], KALPANA CHAUDHARY[2*]

J. Electrical Systems 18-3 (2022): 406-420

Regular paper

Design Enhancement and Comparative Analysis of Low Torque Ripple Double-Stator Switched Reluctance Motor

This paper presents the comprehensive design enhancement and comparative analysis of a low torque ripple double-stator switched reluctance motor for industrial applications. The Double-stator switched reluctance motor (DSSRMs) are gaining popularity due to their high torque density than the conventional tooth switched reluctance motor (TSRM). The main limiting performance parameter for such motors to be adapted for industrial application is their high torque ripple. The design methodology of an improved 12/10 pole DSSRM has already been reported which has the characteristics of very low torque ripples in a wide speed range. However, its detailed comparative analysis with other motors has not been described in the previous literature. This paper further investigates the comparative analysis of this improved motor with the baseline DSSRM and conventional TSRM with the help of 2D finite-element analysis. Comparison is done in the context of average torque, torque ripple, iron and copper weight requirement, harmonic analysis of torque ripple frequency, losses and efficiency. Simulation results confer the effectiveness of improved DSSRM over other two machines.

Keywords: Double-stator switched reluctance motor (DSSRM), finite-element analysis (FEA), torque ripple.

1. Introduction

The Switched reluctance motors (SRMs) are preferred in industrial applications where simple and rugged structure, absence of permanent magnet, fault-tolerance ability, wider-speed range and lower cost are required [1]-[3]. With the advancement in digital signal processors, the control flexibility of SRMs has further improved [4]. The unipolar current excitation permits the use of low-cost converters for SRMs with only single controllable switch per phase [5], [6]. The literature review discusses the ability of SRMs for various applications such as electromotive applications [7], agricultural uses [8], aerospace applications [9] and household instrumentations [10], [11]. Conventional SRMs have the issues of lower efficiency, high torque pulsation; and low torque and power densities. In the literature, several research articles have been reported to enhance these performance indices. In [12], it is reported that a rotor with a segmented structure improves the output torque for the same outer diameter. In [13], it is reported that segmental rotor structure with single-tooth winding topology has improved flux-linkage than full-pitched winding topology, which significantly improves its torque density. Using high-quality iron steel and a higher slot filling can improve efficiency by up to 6% [14]. A control strategy for the switching of the asymmetric half-bridge converter switches is presented in [15] which reduces the switching losses and improves output torque. Researchers have reported several techniques in the literature to mitigate the torque ripple for different topology SRMs. A passive method of torque ripple reduction technique refers to the structural optimization of a machine to mitigate the torque ripple. To reduce the torque ripple in a TSRM, the

* Corresponding author: Kalpana Chaudhary, Department of Electrical Engineering, Indian Institute of Technology (BHU), Varanasi-221005, India, E-mail: kchaudhary.eee@iitbhu.ac.in
[1] Department of Electrical and Electronics Engineering, Nalanda College of Engineering, Nalanda-803108, India
[2] Department of Electrical Engineering, Indian Institute of Technology (BHU), Varanasi-221005, India

modification in the structure of leading-edge rotor poles is introduced in [16]. In the active method of torque ripple reduction technique, the phase currents are given a particular wave shape to reduce the torque ripple. An active method of torque ripple minimization technique through current profiling is reported in [17]. Increasing the phase numbers can also reduce the ripples in torque. To reduce the torque ripple in a six-phase SRM, a torque control methodology with a new six-switch converter is proposed in [18]. A simple control technique to reduce the torque ripple and radial displacement in a single-winding bearingless SRM is introduced in [19]. An ant colony optimization-based speed control methodology to minimize the torque ripple and steady-state speed error is presented in [20] for SRM drives. DSSRM which houses a segmented rotor between two stators further increases torque and power density. In [21], it is reported that DSSRMs can achieve nearly same torque density as interior PM motors but has a lower efficiency and a higher torque ripple. Many torque ripple mitigation techniques which are used for tooth and segmented rotor SRMs can also be applied to DSSRMs. A novel rotor shape optimization is proposed in [22] by drilling four holes in the rotor of a DSSRM for the reduction of torque ripples. Optimization of the stator pole and rotor segment arc angles is introduced via static parametric analysis to obtain a high output torque and low torque ripple in a 12/8 pole DSSRM [23]. The angular displacement of the adjacent rotor segments in opposite directions in a segmented dual-rotor axial-flux SRM can reduce its torque ripple [24]. Similarly, in a double-sided axial-flux tooth SRM, the displacement of adjacent rotor poles in opposite directions reduces the torque ripple, however, a small unbalance axial force is created in the machine [25]. The torque ripple mitigation method with the angular displacement of alternate rotor segments in a 12/10 pole and 24/20 pole radial-flux DSSRMs is discussed in [26]. The torque ripple reduction techniques through the stator and rotor surface shifts; and their affects on motor performance are discussed for DSSRM in [27].

In Ref. [28], the design methodology of an improved 12/10 pole DSSRM is introduced which has very low torque ripple characteristics by angularly shifting the outer stator with half of the stroke angle compared to the inner stator. The respective phase windings of the inner and outer stator are excited parallelly with the same phase shift. The rotor segments are constructed with a pair of half-rotor segments and are isolated from each other with the placement of a wider non-magnetic region between them. The finite-element analysis reveals that the torque ripple is significantly reduced over a wide speed range in the improved machine. However, its detailed comparative analysis with the other motors is missing in that paper. This paper further investigates the effectiveness of that improved motor with the baseline DSSRM and conventional TSRM. A detailed comparative analysis of these motors is carried out with the help of 2D finite-element analysis in this paper. The comparative analysis is done in the context of torque ripple, average torque, torque to weight ratio, efficiency, losses and the harmonic analysis of torque ripple frequencies.

The paper is organised in the following manner: Section 2 deals with the constructional details of the baseline DSSRM and the improved DSSRM. Section 3 deals with the finite-element analysis and the simulation results of the improved DSSRM. Section 4 deals with the comparative analysis of these motors. Finally, Section 5 reveals the conclusions.

2. DSSRM Topology

This section deals with the structural details of a 3-phase 12/10 pole baseline DSSRM as well as of the improved DSSRM which has been proposed in [28]. Fig. 1 represents the diagram of the baseline DSSRM. As the name suggests, the rotor is consist of 10 similar and equally spaced segments which are isolated from each other and sandwiched between two stators. Each stator has a total of 12 poles with alternate thick and thin poles which are pronounced as the exciting and auxiliary poles, respectively. The phase windings considered are in a single-tooth winding configuration, which inherits the advantages of flux cancelling characteristics of inner and outer stator phase coils [21]. The exploded and the cross-sectional views of the baseline DSSRM are represented in Figs. 1(a) and 1(b), respectively. Table 1 includes the design specifications of the baseline DSSRM considered in [28] for FEM analysis. Fig. 2 represents the design parameters graphically. The steady-state response of this motor is simulated at 1000 rpm rated speed for the given specifications. The average torque and torque ripples are 33.6 N-m and 123.8% respectively, which shows the existence of a high torque ripple in this motor.

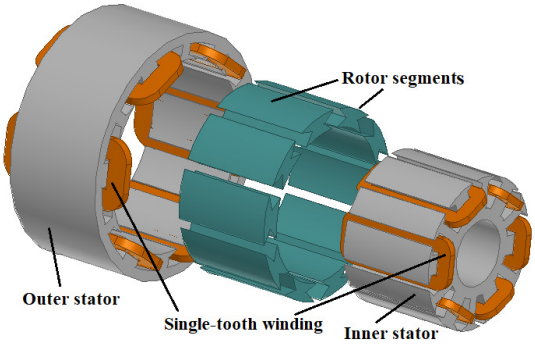

(a)

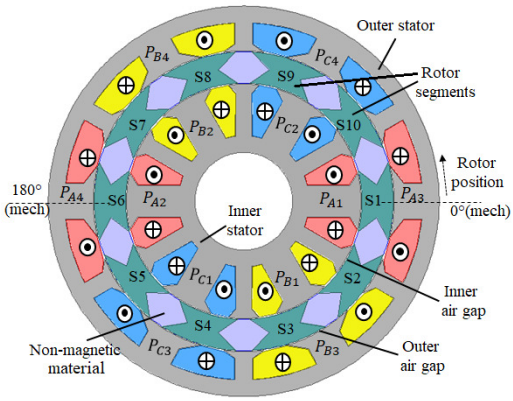

(b)

Figure 1: 3-phase 12/10 pole baseline DSSRM. (a) Exploded view. (b) Cross-sectional view.

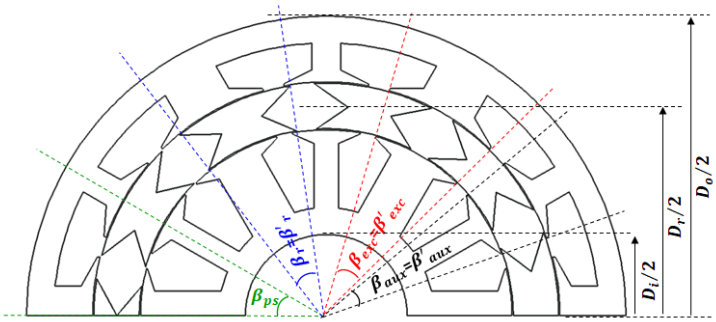

Figure 2: Design parameters of 12/10 pole baseline DSSRM.

Table 1: Design specifications of the baseline DSSRM [28].

Number of the stator pole/rotor segment	12/10
Inner and outer diameters of outer stator	154 and 200 mm
Inner and outer diameters (shaft diameter) of inner stator	50 and 120 mm
Rotor segments height	16 mm
Inner and outer stator yoke height	8.5 mm
Axial length (l)	90 mm
Outer and Inner arc angle of rotor segments (β_r and β'_r)	30°
Auxiliary and exciting pole arc angle (β_{exc}, β_{aux}) of inner stator	15° and 27°
Auxiliary and exciting pole arc angle (β'_{exc}, β'_{aux}) of outer stator	15° and 27°
Stator pole and rotor segment pitch angle (β_{ps}, β_{pr})	30° and 36°
Air gaps length (l_g)	0.5 mm
The Numbers of conductors/slot (N_{slot})	54
The rated power of the motor	3.5 kW
The rated speed of the motor	1000 rpm
The phase current (peak)	30 A
The phase resistance (R)	0.493 Ω
Number of strokes per revolution and stroke angle	30 and 12°

To reduce the torque ripple in DSSRM, first, a hypothetical DSSRM is discussed in [28] which has very low torque ripple characteristics. Fig. 3 shows the FEM model of the hypothetical DSSRM. All the dimensions of the hypothetical DSSRM are the same as in the baseline DSSRM, however, the outer stator has an angular shift of 6° as compared to the inner one. The rotor segments are divided into two parts, namely half-rotor segments, and a hypothetical boundary is inserted between them to completely isolate the inner and outer stator magnetic fluxes. The coils of the inner and outer stator poles of the same phase are excited parallelly with the same phase shift of 6°. The steady-state response of the hypothetical DSSRM is simulated at the rated speed of 1000 rpm and presented in [28]. The average torque and torque ripple are 33.5 N-m and 30.4% respectively. This shows the significantly reduced torque ripple as compared to the baseline DSSRM.

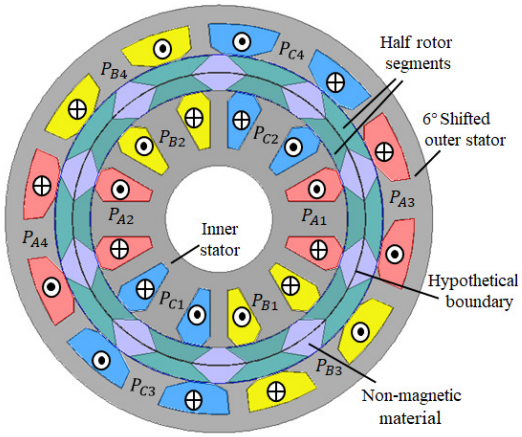

Figure 3: FEM model of the hypothetical DSSRM.

The implementation of the hypothetical DSSRM discussed above is not possible because of the non-existence of such hypothetical boundary in reality. Therefore, the design methodology of an improved DSSRM has been proposed in [28], which has a nearby response as in hypothetical DSSRM. Fig. 4 shows the FEM model of the improved DSSRM. In this model, to achieve a nearby property of the hypothetical boundary, a wider non-magnetic region of the width w_{ins} is inserted between the half-rotor segments, which provides considerable magnetic isolation between inner and outer magnetic circuits. However, the insertion of w_{ins} alters the dimensions and the magnetic property of the outer SRM. This deviates the performance of DSSRM considerably as compared to hypothetical DSSRM. Therefore, the calculation of the optimal values of the design parameters is essential to achieve the nearby characteristics as in hypothetical DSSRM. The required calculations are as listed below:

i. Calculation of the optimal width of the non-magnetic region (w_{ins}).
ii. Calculation of the optimal height of the outer stator poles.
iii. Calculation of the optimal arc angles of the outer half-rotor segments/outer stator poles.

The methodology to calculate the optimal values of these parameters is discussed in [28]. The optimal values of these parameters are listed in Table 2. The performance of the improved DSSRM and its comparative analysis with other machines are discussed in this paper using these optimized values in further sections.

Table 2: Optimal values of the design parameters of improved DSSRM.

Optimal width : Non-magnetic region (w_{ins})	12.5 mm
Optimal height : Outer stator poles	11.5 mm
Optimal arc angles : Outer rotor segments / stator poles (β'_r , β'_{exc} , β'_{aux})	27.84°, 26.48°, 14.12°
Outer diameter of motor	219 mm

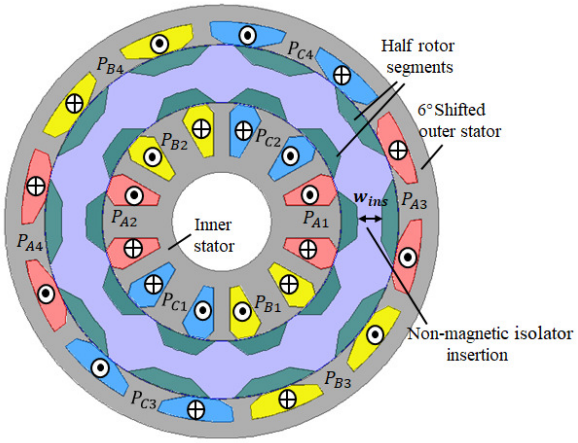

Figure 4: FEM model of the improved DSSRM.

3. Finite-element analysis and simulation results

Table 2 enlists the values of some optimized design parameters of the improved DSSRM after modifications. Rest of the specifications are as listed in Table 1. Concerning its very high accuracy for radial-flux machines, the 2-D FEM analysis has proceeded to obtain the static and dynamic electromagnetic characteristics of the machine in ANSYS/MAXWELL environment. To achieve the dynamic response asymmetric half-bridge converter is used which requires two switches per phase. Asymmetric half-bridge converters are very popular because of their control flexibility [29]. The phase currents are limited around the reference value using the hysteresis control technique with a band of ±0.5 A. To calculate the core losses 0.4 mm thickness is considered for the laminations. The phase conduction period considered is 143° (elec.) for the rated speed of 1000 rpm with the turn-on angle of 0°. The governing equations to calculate the % torque ripple (T_{ripple}) and % efficiency (η) are given in Eq. (1) and Eq. (2) respectively, where T_{pk-pk} is peak-to-peak torque ripple, T_{avg} is average output torque, P is the mechanical output power, P_i is the iron or core loss and P_{cu} is the copper loss.

$$T_{ripple} = (T_{pk-pk}/T_{avg}) \times 100 \tag{1}$$

$$\eta = P/(P + P_i + P_{cu}) \times 100 \tag{2}$$

Fig. 5 shows the static torque profiles of the inner and outer stator windings of the improved DSSRM. The torque profiles are calculated through the parametric analysis of stator winding currents between 5A to 30A with a step size of 5A. It can be seen that the torque waveforms of the outer stator are somehow more peaky than the inner one for the same current. This will add some peaky response in the dynamic torque output. Fig. 6 shows the dissemination of the flux density in the different parts of the improved DSSRM model at 90° and 150° (elec.) rotor positions for rated condition. The steady-state response of the improved machine is simulated at the rated speed and its phase currents and torque waveform are presented in Fig. 7. In the figure; i_a, i_b, i_c and $i_{a'}$, $i_{b'}$, $i_{c'}$ are the respective phase currents of the inner and outer stator windings. The values of the average torque and torque ripple are 33.7 N-m and 31.1%, respectively. The core and copper losses are 109 W

and 370 W respectively, therefore the rated efficiency is 88.0%. The total active weight of the machine is 15.6 kg resulting in the torque to active weight ratio of 2.16 N-m/kg. Thus it can be revealed that the improved machine has a high value of torque density and efficiency with a significantly low value of torque ripple at the rated operating condition.

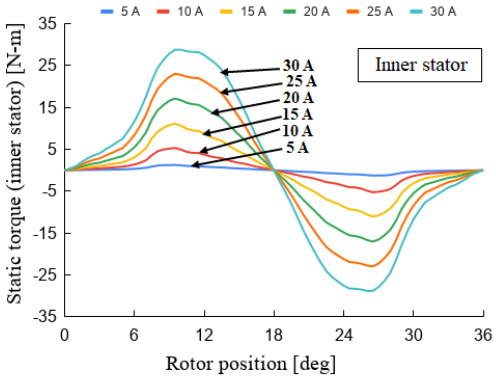

(a)

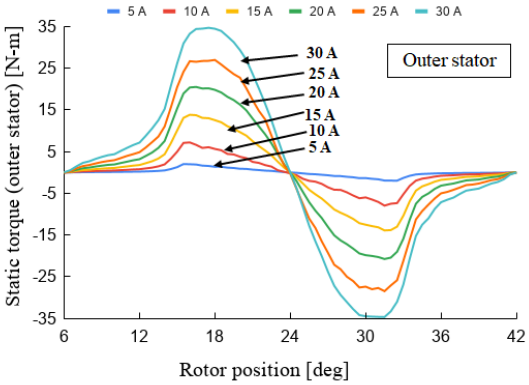

(b)

Figure 5: Static torques of inner and outer stator windings. (a) Inner stator winding. (b) Outer stator winding.

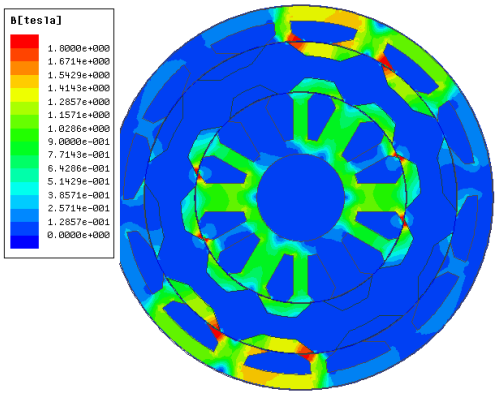

(a)

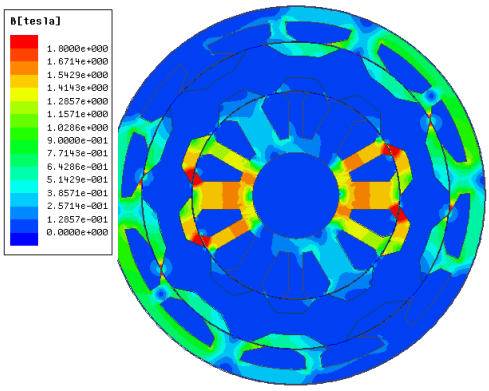

(b)

Figure 6: Dissemination of flux density in the improved DSSRM at rated condition. (a) Flux density at 90° (elec.) rotor position. (b) Flux density at 150° (elec.) rotor position.

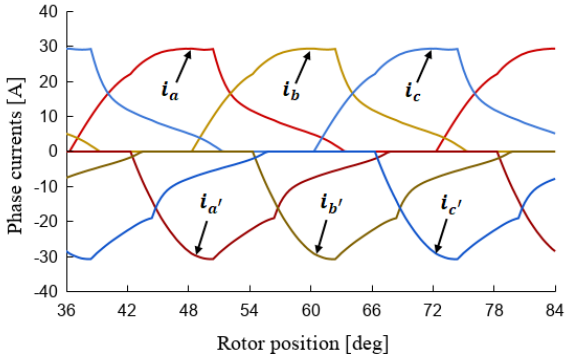

(a)

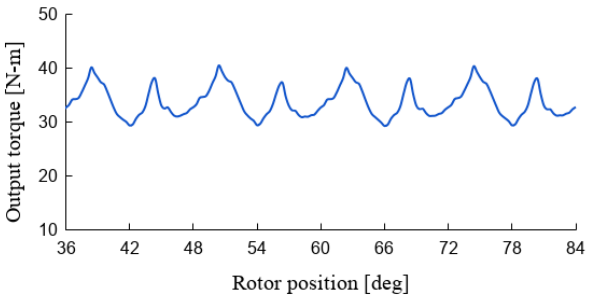

(b)

Figure 7: Steady-state response of improved DSSRM at 1000 rpm. (a) Phase current waveforms. (b) Torque waveform.

4. Comparative analysis of the improved DSSRM with other motors

In this section, the comparative analysis of the improved DSSRM is performed with the baseline DSSRM and a 12/8 pole conventional TSRM to inspect its suitability over the other two motors. For this, the FEM models of the baseline DSSRM and TSRM have also been modelled and their performances are simulated. During modelling, the slot fill factor

(SFF) is considered same in each case which is 43%. The average current density is also considered nearly same in each case which is nearly 5.5 A/sq. mm. The outer diameter considered is 200 mm for baseline DSSRM and TSRM, however, it is somehow higher for improved DSSRM due to the insertion of w_{ins} between half-rotor segments, which is 219 mm. The axial lengths are varied to obtain the rated torque at the rated speed. The axial length is 90 mm for baseline and improved DSSRM, whereas for TSRM this length requirement increases to 134 mm. The dynamic responses of these motors are simulated considering same phase conduction period (elec. deg.) with same turn-on and turn-off angles for each motor. The steady-state torque waveforms of these motors are drawn in Fig. 8 (a) for the rated speed of 1000 rpm. The average torque is comparable in each case. The torque ripples for improved DSSRM, baseline DSSRM and TSRM are 31.1%, 123.8% and 97.0%, respectively. Thus it can be divulged that torque ripple is significantly reduced in the improved DSSRM as compared to the other two machines. Some design and performance data are tabulated in Table 3. It can be seen that the core loss is high in the improved DSSRM as compared to the baseline DSSRM due to the increase in leakage flux between half-rotor segments near unaligned rotor position. Moreover, the copper loss has a lower value in the improved DSSRM as compared to baseline DSSRM because of the lower rms current requirement in it for the same torque generation. In the case of TSRM, the core loss is high due to its higher axial length. The rated efficiency and torque to active weight ratio are comparable for improved and baseline DSSRMs, however, these values reduce in the case of TSRM due to the increase in core loss and higher axial length requirement.

Table 3: Comparative data for improved/baseline DSSRMs and 12/8 pole TSRM at rated speed.

	Improved DSSRM	Baseline DSSRM	TSRM
Outer diameter in mm	219	200	200
Axial length in mm	90	90	134
Rotor speed in rpm	1000	1000	1000
Turn-on angle (elec. deg.)	0	0	0
Turn-off angle (elec. deg.)	143	143	143
T_{avg} in N-m	33.7	33.6	33.8
T_{pk-pk} in N-m	10.5	41.6	32.8
T_{ripple} in %	31.1	123.8	97.0
Constant loss (P_i) in W	109	93	124
Variable loss (P_{cu}) in W	370	385	384
Rated % efficiency	88.0	88.0	87.4
Total active weight in kg	15.6 (102.6%)	15.2 (100%)	21.9 (144.1%)
Active weight ratio torque in N-m/kg	2.16 (97.7%)	2.21 (100%)	1.54 (69.7%)

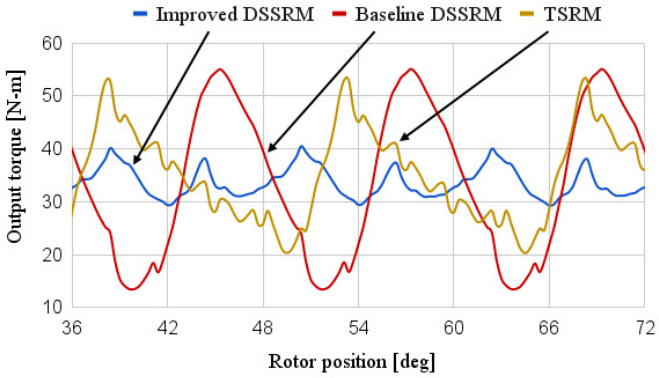

(a)

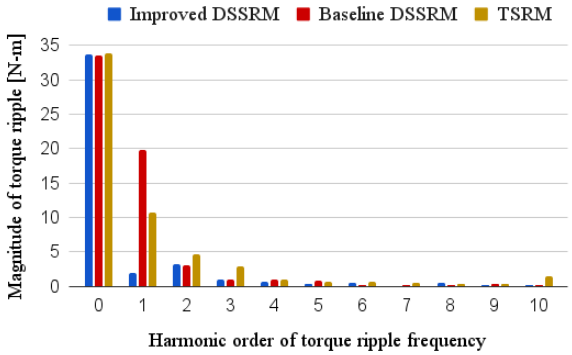

(b)

Figure 8: Comparison of the steady-state torques of different machines at the rated speed of 1000 rpm. (a) Steady-state torques. (b) Magnitude of torque ripple harmonics.

Fig. 8 (b) inculcates the harmonic analysis of torque ripple frequencies of the motors for rated speed. 12/10 pole motors which are improved and baseline DSSRMs have 30 strokes per revolution, therefore for 1000 rpm speed their fundamental torque ripple frequency is 500 Hz. However, 12/8 pole TSRM has 24 strokes per revolution, therefore it has a fundamental torque ripple frequency of 400 Hz for the same speed. The figure represents the magnitude of the torque ripples up to the 10th harmonic order for the rated speed. The average or DC values are 33.7 N-m and 33.6 N-m for improved and baseline DSSRM, respectively, as well as 33.8 N-m for TSRM. These values are 2.0 N-m, 19.8 N-m and 10.7 N-m for the fundamental frequency which is the most dominant harmonic. Thus it can be revealed that the lower-order torque ripples are significantly reduced in improved DSSRM.

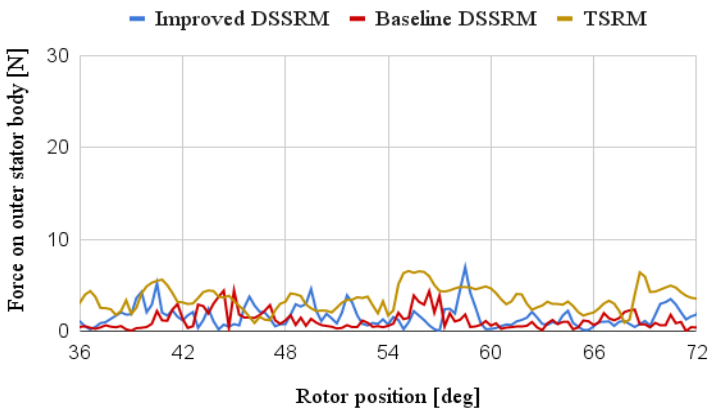

Figure 9: Resultant force on the outer stator body of the motors.

Fig. 9 represents the instantaneous force resulting on the outer stator body for all three motors at rated speed. The average values of these forces are 1.6 N, 1.3 N and 3.6 N, respectively for improved DSSRM, baseline DSSRM and TSRM, which are ignorable. Thus it can be concluded that the modifications in the improved DSSRM do not create any unbalance force on it.

The performance comparison of these motors is further extended below and above the rated speed and the results are shown in Fig. 10. Below the rated speed, the constant torque operation is achieved by controlling the phase current via the hysteresis current control method. Furthermore, above the rated speed, the output power is maintained constant by advancing the phase turn-on angle before the rated turn-on value [30]. Fig. 10 (a) represents the torque-speed characteristics of these motors by employing the above control techniques. It can be seen that the output torque has nearly constant value below the rated speed for each motor. Similarly, the output power is also nearly constant above the rated speed for each motor. Fig. 10 (b) represents the torque ripples of these motors with the variation of rotor speed. It is seen that the torque ripples are sufficiently low in the improved DSSRM as compared to the baseline DSSRM and TSRM in all speed range. There is a very small variation in torque ripple over a wide speed range in the improved DSSRM, especially between 800 rpm to 1400 rpm, where it is maintained between 27.1% to 34.1%. It is observed that TSRM has comparatively low torque ripple in most of the speed range as compared to the baseline DSSRM, however, it has still sufficiently high torque ripple values as compared to the improved DSSRM. Fig. 10 (c) shows the variation of core loss in all three machines with the variation of rotor speed. It can be seen that core loss increases in each machine with the increase in rotor speed. This is because the frequency of flux variation increases with the increase in rotor speed. Moreover, this figure also shows that the core losses are comparatively high in TSRM because of the requirement of a higher axial length for the same torque generation. The figure also depicts that the improved DSSRM attains higher core loss as compared to baseline DSSRM. This is because of the increase in leakage flux between the half-rotor segments near unaligned rotor position. The improved DSSRM and TSRM have respectively 17.2% and 33.3% more core loss as compared to baseline DSSRM at rated speed. Fig. 10 (d) represents the variation of copper loss with the rotor speed. It can be observed that even though the TSRM has a higher value

of axial length, it has a comparable copper loss as the other two machines, because of nearly same copper weight requirement in all three machines. Fig. 10 (e) represents the weights of the iron and copper materials as well as the total active weights of these machines. Because of the higher axial length, the iron weight increases in TSRM which increases its total active weight and reduces its torque to active weight ratio. The copper weight is nearly same in all three machines, which endorses that the DSSRMs attain a higher value of torque density by allowing higher copper volume as compared to conventional TSRMs. Fig. 10 (f) represents the variation of efficiency with the rotor speed. It can be seen that in lower speed region up to 800 rpm the efficiency of all three motors is nearly equal. However, with the further increase in speed, the efficiency of DSSRMs slightly increases as compared to TSRM. This shows the efficacy of DSSRM over TSRM in high-speed operation.

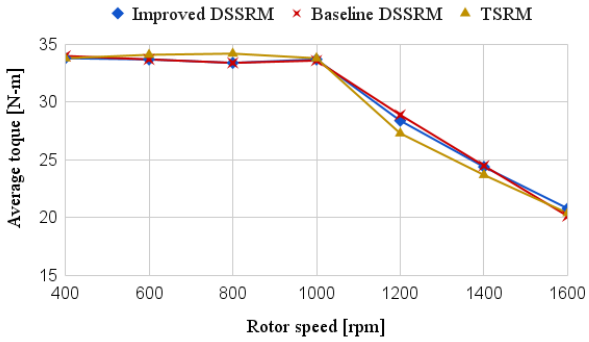

(a)

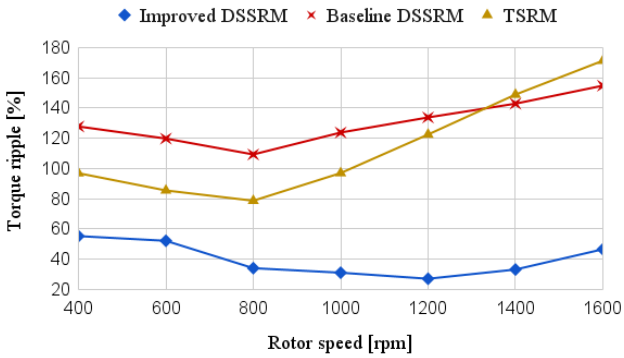

(b)

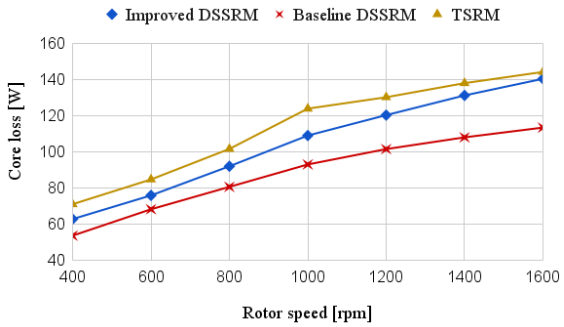

(c)

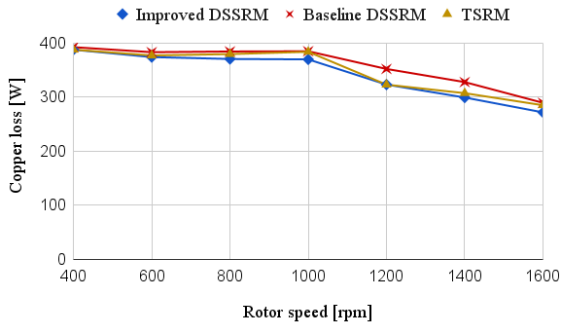

(d)

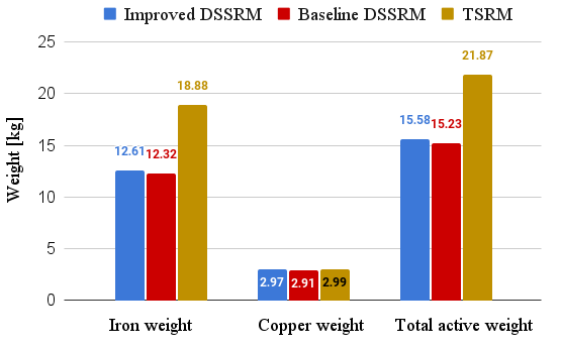

(e)

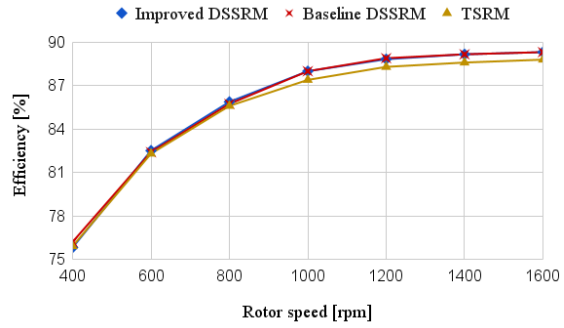

(f)

Figure 10: Comparison of the performance parameters at different rotor speed. (a) Average torque. (b) Torque ripple. (c) Core loss. (d) Copper loss. (e) Required iron and copper

weights. (f) Efficiency.

5. Conclusion

DSSRMs have high torque density compared to conventional TSRMs. However, they have high torque ripple. In the literature, the design methodology of an improved 12/10 pole DSSRM has been proposed which has a very low torque ripple characteristics over a wide speed region. However, its comparative analysis with other motors is missing in the literature. This paper further investigates the comparative analysis of the improved DSSRM with the baseline DSSRM and conventional TSRM with the help of 2D finite-element analysis. Comparison is done in the context of average torque, torque ripple, iron and copper weight requirement, harmonic analysis of torque ripple frequency, losses and efficiency. During modelling, the same slot-fill factor and same average current density are considered in all three machines, however, axial lengths are varied to obtain the rated torque. Simulation results conclude that the improved DSSRM has significantly low torque ripple in a wide speed region, especially between 800 rpm to 1400 rpm, where it is maintained between 27.1% to 34.1%. These values for baseline DSSRM are between 109.3% to 142.9%, and for TSRM between 78.7% to 148.9%. Core loss is slightly high in improved DSSRM compared to baseline DSSRM due to the increase in leakage flux, but maximum in TSRM due to the increase in axial length requirement. Copper loss is slightly low in improved DSSRM and TSRM due to a slightly lower rms phase current value. The efficiency is comparable in all three machines in low-speed region but slightly increases in DSSRMs in high-speed region. It is observed that even though the DSSRMs have lower axial length, all three machines require same copper weight to generate the rated torque. This concludes that the DSSRMs attain a higher torque density by allowing higher copper volume compared to conventional TSRMs. The harmonic analysis of torque ripples concludes that the magnitudes of the low-frequency torque ripples are significantly low in improved DSSRM. The fundamental harmonic is 6.0% of DC value in improved DSSRM, while this value in baseline DSSRM and TSRM are 59.0% and 31.7%, respectively.

References

[1] A. Chiba, K. Kiyota, N. Hoshi, M. Takemoto and S. Ogasawara, Development of a Rare-Earth-Free SR Motor With High Torque Density for Hybrid Vehicles, *IEEE Transactions on Energy Conversion*, *30*(1), 175-182, 2015.

[2] D. Gerada, A. Mebarki, N. L. Brown, C. Gerada, A. Cavagnino and A. Boglietti, High-Speed Electrical Machines: Technologies, Trends, and Developments, *IEEE Transactions on Industrial Electronics*, *61*(6), 2946-2959, 2014.

[3] A. G. Jack, B. C. Mecrow and J. A. Haylock, A comparative study of permanent magnet and switched reluctance motors for high-performance fault-tolerant applications, *IEEE Transactions on Industry Applications*, *32*(4), 889-895, 1996.

[4] P.Srinivas and P.V.N.Prasad, DSP based Speed Control of 4 phase 8/6 Switched Reluctance Motor Drive using DC Split Converter, *Journal of Electrical Systems*, *8*(1), 47-56, 2012.

[5] Q. Sun, J. Wu, C. Gan, Y. Hu, N. Jin, and J. Guo, A new phase current reconstruction scheme for four-phase SRM drives using improved converter topology without voltage penalty, *IEEE Trans. Ind. Electron.*, *65*(1), 133–144, 2018.

[6] R. Krishnan, Sung-Yeul Park and Keunsoo Ha, Theory and operation of a four-quadrant switched reluctance motor drive with a single controllable switch-the lowest cost four-quadrant brushless motor drive, *IEEE Transactions on Industry Applications*, *41*(4), 1047-1055, 2005.

[7] R. Madhavan and B. G. Fernandes, Axial Flux Segmented SRM With a Higher Number of Rotor Segments for Electric Vehicles, *IEEE Transactions on Energy Conversion*, *28*(1), 203-213, 2013.

[8] A. K. Mishra and B. Singh, Self-governing single-stage photovoltaic water pumping system with voltage balancing control for a four-phase SRM drive, *IET Electric Power Applications*, *14*(1), 119-130, 1 2020.

[9] J. Borg Bartolo, M. Degano, J. Espina and C. Gerada, Design and Initial Testing of a High-Speed 45-kW Switched Reluctance Drive for Aerospace Application, *IEEE Transactions on Industrial Electronics*, *64*(2), 988-997, 2017.

[10] J. Liang, L. Jian, G. Xu, and Z. Shao, Analysis of electromagnetic Behavior in switched reluctance motor for the application of integrated air conditioner on-board charger system, *Progress in Electromagnetics Research*, *124*, 347-364, 2012.
[11] K. Isobe, K. Nakamura, and O. Ichinokura. A consideration of High Speed SR Motor for Electric Power Tools, *Journal of the Magnetics Society of Japan*, *38*(5), 194-198, 2014.
[12] B. Mecrow, J. Finch, E. El-Kharashi, and A. Jack, Switched reluctance motors with segmental rotors, *IEE Proc.—Electric. Power Appl.*, *149*(4), 245–254, 2002.
[13] B. C. Mecrow, E. A. El-Kharashi, J. W. Finch and A. G. Jack, Segmental rotor switched reluctance motors with single-tooth windings, *IEE Proceedings - Electric Power Applications*, *150*(5), 591-599, 2003.
[14] H. Hayashi, K. Nakamura, A. Chiba, T. Fukao, K. Tungpimolrut, and D. Dorrell, Efficiency improvements of switched reluctance motors with high-quality iron steel and enhanced conductor slot fill, *IEEE Trans. Energy Convers.*, *24*(4), 819–825, 2009.
[15] Slamet Riyadi, A Control Strategy for SRM Drive to Produce Higher Torque and Reduce Switching Losses, *Journal of Electrical Systems*, *14*(4), 205-216, 2018.
[16] Li, Y.; Ravi, S.; Aliprantis, D.C., Tooth Shape Optimization of Switched Reluctance Motors for Improved Torque Profiles, *Power & Energy Society General Meeting*, pp.1-7, 26-30, 2015.
[17] R. Mikail, I. Husain, Y. Sozer, M. S. Islam, and T. Sebastian, Torque ripple minimisation of switched reluctance machines through current profiling, *IEEE Trans. Ind. Appl.*, *49*(3), 1258–1267, 2013.
[18] X. Deng, B. Mecrow, H. Wu and R. Martin, Design and Development of Low Torque Ripple Variable-Speed Drive System With Six-Phase Switched Reluctance Motors, *IEEE Transactions on Energy Conversion*, *33*(1), 420–429, 2018.
[19] X. Cao, J. Zhou, C. Liu and Z. Deng, Advanced Control Method for a Single-Winding Bearingless Switched Reluctance Motor to Reduce Torque Ripple and Radial Displacement, *IEEE Transactions on Energy Conversion*, *32*(4), 1533-1543, 2017.
[20] Mohamed Yaich and Moez Ghariani, Control Strategy for Switched Reluctance Motor Based on Embedded System, *Journal of Electrical Systems*, *14*(1), 156-173, 2018.
[21] E. Bostanci, M. Moallem, A. Parsapour, and B. Fahimi, Opportunities and challenges of switched reluctance motor drives for electric propulsion: A comparative study, *IEEE Trans. Transport. Electrific.*, *3*(1), 58-75, 2017.
[22] M. A. Tavakkoli and M. Moallem, Torque ripple mitigation of double stator switched reluctance motor (DSSRM) using a novel rotor shape optimisation, *IEEE Energy Conversion Congress and Exposition (ECCE)*, Raleigh, NC, 2012, pp. 848-852.
[23] Q. Sun, J. Wu, C. Gan, C. Shi and J. Guo, DSSRM Design With Multiple Pole Arcs Optimization for High Torque and Low Torque Ripple Applications, *IEEE Access*, *6*, 27166-27175, 2018.
[24] R. Madhavan and B. G. Fernandes, Performance Improvement in the Axial Flux-Segmented Rotor-Switched Reluctance Motor, *IEEE Transactions on Energy Conversion*, *29*(3), 641–651, 2014.
[25] M. J. Kermanipour and B. Ganji, Modification in Geometric Structure of Double-Sided Axial Flux Switched Reluctance Motor for Mitigating Torque Ripple, *Canadian Journal of Electrical and Computer Engineering*, *38*(4), 318–322, 2015.
[26] T. D. Gupta, K. Chaudhary, R. M. Elavarasan, R. K. Saket, I. Khan and E. Hossain, Design Modification in Single-Tooth Winding Double-Stator Switched Reluctance Motor for Torque Ripple Mitigation, *IEEE Access*, *9*, 19078-19096, 2021, doi: 10.1109/ACCESS.2021.3052828.
[27] T. D. Gupta and K. Chaudhary, Research on Torque Ripple Minimization of Double-stator Switched Reluctance Motor Using Finite Element Method, *Advances in Electrical and Computer Engineering, 21*(4), 135-144, 2021.
[28] T. D. Gupta and K. Chaudhary, Finite Element Method Based Design and Analysis of a Low Torque Ripple Double-Stator Switched Reluctance Motor, *Progress in Electromagnetics Research C*, *111*, 191-206, 2021.
[29] T. J. E. Miller, Switched Reluctance Motors and Their Control. London, U.K.: CRC Press, 1993.
[30] M. Rekik, M. Besbes, C. Marchand, B. Multon, S. Loudot and D. Lhotellier, Improvement in the field-weakening performance of switched reluctance machine with continuous mode, *IET Electric Power Applications*, *1*(5), 785-792, 2007.